Prediction of Hysteretic Matric Potential Dynamics Using Artificial Intelligence: Application of Autoencoder Neural Networks

Nedal Aqel[1], Lea Reusser[1,2,3], Stephan Margreth[2], Andrea Carminati[1], and Peter Lehmann[1]*

[1]*Physics of Soils and Terrestrial Ecosystems , ETH Zurich, Switzerland*
[2]*Office for the Environment, canton of Solothurn, Switzerland*
[3]*now at the Swiss Academy of Sciences, Forum Landscape, Alps, Parks (FoLAP), Switzerland*

*Corresponding author, nedal.aqel@usys.ethz.ch, Universitätstrasse 16, 8092 Zurich, Switzerland

Abstract

Information on soil water potential is essential to assess soil moisture state, to prevent soil compaction in weak soils, and to optimize crop management. In lack of direct measurements, the soil water potential values must be deduced from soil water content dynamics that can be monitored at plot scale or obtained at larger scale from remote sensing information. Because the relationship between water content and soil water potential in natural field soils is highly ambiguous, the prediction of soil water potential from water content data is a big challenge. The hysteretic relationship observed in nine soil profiles in the region of Solothurn (Switzerland) is not a simple function of texture or wetting and drainage cycles but depends on seasonal patterns that may be related to soil structural dynamics. Because the physical mechanisms governing seasonal hysteresis are unclear, we developed a deep neural network model that predicts water potential changes using rainfall, potential evapotranspiration, and water content time series as inputs. To adapt the model for multiple locations, we incorporated a Deep Autoencoder Neural Network as a classifier. The autoencoder compresses the water content time series into a site-specific feature that is highly representative of the underlying water content dynamics of each site and quantifies the similarity of dynamic patterns. By adding the Autoencoder's output as an additional input and training the neural network model with three stations located in three major classes founded by the autoencoder, we predict matric potential for other sites. This method has the potential to deduce the dynamics of matric potential from water content data (including satellite data) despite strong seasonal effects that cannot be captured by standard methods.

1. Introduction

The soil water characteristics curve SWC relates the matric potential (MP) and water content (WC) and is the key physical property to quantify soil water dynamics (Tuller & Or, 2023). The SWC (also denoted as soil water retention curve or pressure-saturation relationship) depends on both soil texture and structure and differs with soil types and soil textural classes (Rawls, et al., 2003; Shwetha & Varija, 2015). The SWC contains information on the pore size distribution and allows the assessment of flow and transport properties for different hydration states (Rostami, et al., 2015; Menon, et al., 2020). To provide a complete characterization of the actual soil moisture state and flow regimes, information on both the matric potential and the water content must be specified. Information on volumetric water content is needed to assess the free storage capacity, optimize water management, and to formulate mass balance. The matric water potential is a component of the total and hydraulic soil water potential and determines the water flow in direction of decreasing water potential to achieve equilibrium with its surroundings (Ma, et al., 2022). The matric potential is also of particular interest to assess mechanical stability of a soil (Holthusen, et al., 2010; Lu, et al., 2010). The capillary and adsorptive forces expressed with the matric potential define the unsaturated soil strength mitigating soil compaction by heavy machinery in construction work, farming, and forestry (Smith, et al., 2001). For example, matric potential thresholds are defined in various regions of Switzerland to prevent mechanical damage and regulate the maximum load linked to factors like soil type, texture, and vehicle impact (Bundesamt für Energiewirtschaft, 1997). Other important potential thresholds are the wilting point and the field capacity, characterizing the plant available water (Gupta, et al., 2023).

It would be optimal to determine the soil moisture status relative to these potential thresholds based on information of water content using the SWC, without direct measurement of the matric potential. In that case, matric potential dynamics could be deduced from remote sensing water content data that are available at various scales. However, the application of this procedure is limited by two effects. Firstly, under saturated conditions, the water potential can change without modifying the volumetric water content. The transition of conditions with negative water potential within the capillary fringe to positive pressures below a water table is crucial for the triggering of landslides (Gallipoli, et al., 2003). Secondly, the SWC under field conditions is often an ambiguous relationship between potential and water content due to hysteretic and dynamic effect as will be discussed next.

The SWC is typically measured in the lab as series of equilibrium states obtained during drainage, with one water content value assigned to the applied pressure. The results of such small-scale experiments are not sensitive to structural pores that can be found at the field scale (Romero-Ruiz, et al., 2018) and can thus be expressed as function of basic soil properties (texture, bulk density, content of organic material) using pedotransfer functions (PTF; Zuo & He, 2021). Because these PTFs ignore the effects of soil structures including macropores and cracks (Basile, et al., 2019) and are trained with data from small samples with artificially high initial saturation conditions, their applicability to model dynamic processes in the field is limited. Another limitation is the underlying assumption of an unambiguous relationship between water content and matric potential (and hydraulic conductivity). In all land surface models, water content is linked by an unambiguous relationship between water content and matric potential. In reality, this relationship is highly ambiguous under field conditions as was analyzed in detail by Hannes et al. (2016) and as we will show later in this paper as well.

Hannes et al. (2016) analyzed long-term experiments and concluded that the high variation of matric potential values for the same water content are a result of hysteresis, dynamic effects, and structural changes during the season. Hysteresis is related to differences in wetting and drying cycles (Capparelli & Spolverino, 2020) as controlled by different pore structures controlling air- or water invasion and differences in receding or advancing wetting angles (Fomin, et al., 2023). Hysteresis is often manifested in coarse textured soils and occurs as well during slow processes. Another process resulting in an ambiguous pressure-saturation relationship is dynamic effects with water contents that are not in equilibrium with the quickly changing potential (Ross & Smettem, 2000). Finally, the size of structural pores is not constant with time but changes with season, water content, and soil formation processes (Fu, et al., 2021). The combined effect of hysteresis, non-equilibrium, and structural changes makes it extremely challenging to deduce soil matric potential from information on water content. Also, the implementation of these combined effects in physically-based models of unsaturated water flow is not straightforward. As an alternative approach to physically-based models, machine learning can be applied to simulate the complex relationship between matric potential and water content under field conditions. In this study, we will apply a deep neural network (DNN).

Deep neural networks (DNN) have demonstrated their effectiveness as a powerful numerical tool for resolving complex patterns. Their ability to learn from data and recognize intricate relationships makes them valuable in various fields, including the modeling of soil water characteristics. For example, Jain, et al. (2004) and Achieng (2019) used artificial neural network (ANN) models to predict the hysteretic water content from observed matric potential values. However, both publications simulated lab data under equilibrium conditions and cannot be applied for the more complex dynamic processes in the field. In addition, the models were site-specific and needed both water content and matric potential information for the training. Here we will apply a different DNN using an autoencoder approach. As we will explain in the theory section, the autoencoder condenses the complexity of temporal (and spatial) patterns into a single (or a few) number(s). The hypothesis of this study is that the autoencoder value is a new and unique characterization of the soil moisture dynamics and can be used to predict matric potential dynamics from observed water content data. The paper is organized as follows: in section 2, the study sites and the basics of the deep neural network with the autoencoder approach are presented. The results section compares the model performance of site-specific deep neural network (DNN) and shows the possibility to build a generalized DNN using the autoencoder analysis as model input. Limits and possible applications of the model approach are discussed in section 5.

2. Material and methods

In a first step, matric potential time series were simulated at nine sites in the region of Solothurn (Switzerland) using site specific ANN model, to proof that the ANN models can predict matric potential from water content dynamics with site specific training. In the next step, the autoencoder analysis of water content dynamics of all sites was conducted. Finally, the site-specific ANN model was enhanced and transformed into a multisite model by combining two deep neural networks. This transformation allowed for a more comprehensive and versatile predictive framework of matric potential as function of water content.

2.1 Study area and soil moisture data

The study area covers mainly the canton of Solothurn in Switzerland (Fig.1), and thus an area of approximately 629 km^2. The climate in Solothurn is classified as oceanic climate (Cfb) according to Koppen and Geiger climate classification, with an average yearly temperature of 9.5 °C and annual precipitation of around 1400 mm. Approximately half of the annual precipitation in the canton undergoes the process of evaporation (Spreafi & Weingartner, 2005). During the year, the average temperature varies by 19 °C with the highest temperature occurring in the month of July and the lowest average temperature in January. Regarding precipitation patterns, the month of June has the highest level of precipitation, while March stands out as the driest month. Soil moisture dynamics (see below) were studied for the period from 2011 to 2022. For this period, climatic data was available on the data portal of MeteoSwiss (IDAweb, 2024) . The data was gathered from the closest meteorological stations to each of the nine sites in the Solothurn region.

Soil moisture data were downloaded from the 'soil monitoring network' (BODENMESSNETZ, 2024) collecting data from 65 stations distributed over eleven cantons of Switzerland. The network's primary objective is to provide real-time soil moisture information for mitigating soil compaction. BODENMESSNETZ also plays a role in raising awareness among farmers and foresters about soil compaction, providing a tool to assess the current situation and adjust the use of heavy machinery based on weather conditions. As the network has been running since 2011, it now serves as a valuable resource by offering long-term diverse information, including land use, precipitation amounts, and matric potential measured at various depths (20 and 35 cm depth in most of the stations, using T8 and T32 tensiometers from METER group). Only at nine sites that are located in the region of Solothurn, the water content was measured at 20 cm depth (Stevens Hydra Probe). For these nine sites, daily values in volumetric water content (20 cm), matric potential (20 cm) and precipitation values were used. The matric potential in the downloaded data was given in kPa and was transferred to matric potential head with units of cm (1 cm is 0.1 kPa), considering a water density of 1000 kg m^{-3} and gravity acceleration of 10 m s^{-2}.

As the soil moisture decreases, water is drawn from the tensiometer, creating a negative pressure or tension. During dry periods, cavitation may occur, causing water vaporization and air bubble formation (Mendes & Buzzi, 2013), or tensiometers had to be refilled (Sadeghi, et al., 2020). To address these challenges and ensure accurate data collection, various data preprocessing and filtering techniques were implemented. These techniques involved identifying and removing outliers, systematically excluding data points with water potential values within the problematic dry ranges and filtering out data points with extremely low or high water content values. The study also flagged abrupt changes in volumetric water content (VWC) and matric potential (MP) for further investigation, as these could indicate measurement anomalies. Additionally, a thorough analysis of weekly trends in the data was conducted to identify systematic variations over time (see Appendix A).

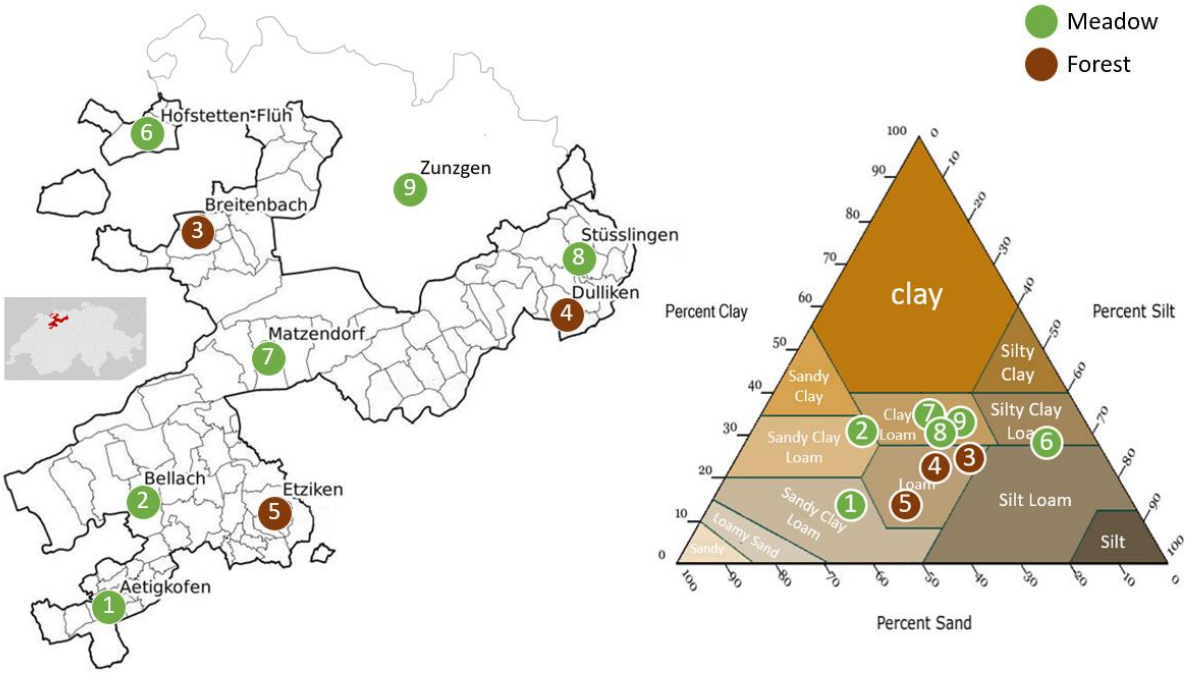

Figure 1 Overview of the study area with site locations, soil texture, and land cover. The primary focus is on the canton of Solothurn, outlined by the black border on the map, with an additional site from the canton of Basel (site 9, Zunzgen). Within this region, three sites are categorized as forests, while the remaining six sites are designated as meadows. The analyzed soil horizons (20 cm depth) of the study area encompasses five soil textural classes as shown in the soil texture triangle.

The analyzed soil horizons of the selected locations can be assigned to five different soil textural classes (figure 1) and two different land covers (meadow and forest). The location denoted as Matzendorf (site #7) contains the highest clay content, whereas locations such as Aetigkofen (site #1) are predominantly sandy. Across these nine locations, different relationships between matric potential and water content were deduced from field data as shown in Figure 2 for two sites with low and high variations in water content for similar potential values. To show the relevance of seasonal patterns, we differentiate between summer (April to September) and winter period (remaining months).

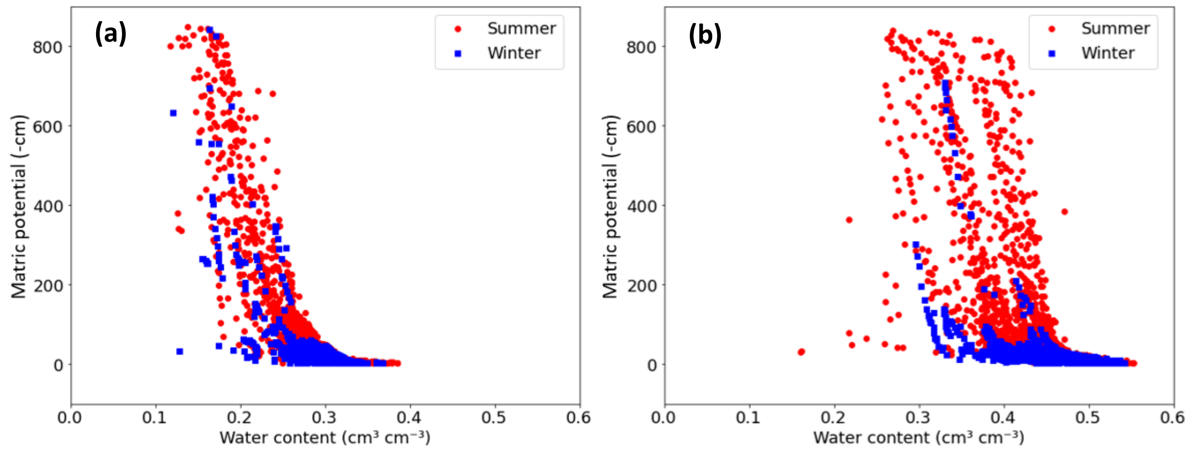

Figure 2 Soil-Water characteristics curve (SWC) measured in the field at two sites classified into summer (April to September) and winter period (remaining months) from 2012 to 2023. **(a)** The Etziken site (site #5) shows small changes in the SWC dynamics over the years, for both the warm and cold period. **(b)** A contrasting scenario was found for the site in Bellach (site #2) that was characterized by a wide range of water content for similar potential values. The unit of matric potential, represented as -cm, is equivalent to -0.1 kPa.

2.2 Deep neural network (DNN)

A basic artificial neural network (ANN) comprises one or two hidden interconnected layers, with each layer tasked with the conversion of an input vector ($\boldsymbol{x}$) into a hidden state vector ($\boldsymbol{h}$), as described by (Bertels & Willems, 2023). This conversion is accomplished with eq. (1):

$$\boldsymbol{h} = f(\boldsymbol{x}) = act(\mathbf{W} \bullet \boldsymbol{x} + \boldsymbol{b}) \quad (1)$$

Where $f(\boldsymbol{x})$ represents the transformation function applied to the input vector($\boldsymbol{x}$), with a weight matrix ($\mathbf{W}$) and a bias vector ($\boldsymbol{b}$), integrated with an activation function (denoted as "act").

To construct a deep neural network (DNN), multiple layers (more than two hidden layers) are interconnected to form a 'multilayer perceptron.' The training process involves finding optimal values for the weights and biases in the network using suitable optimization techniques (Bertels & Willems, 2023). In this study, DNN was built to predict the daily MP for the nine sites. The process involved several key steps. First, in the design of the neural network, activation functions were carefully selected and integrated to introduce non-linearity into the model's transformations (Montesinos Lópezm, et al., 2022). The Rectified Linear Unit (ReLU) activation function was employed to mitigate vanishing gradient problem and enhance the model's ability to handle noisy input. The inclusion of ReLU was motivated by considerations of computational efficiency, with some attention given to the potential issue of "dying ReLU" (Montesinos Lópezm, et al., 2022; Lu, 2020).

Next, the neural network was structured with a total of six layers, including four hidden layers as suggested by Achieng (2019). All layers were densely connected, fostering strong information flow between neurons. Crucially, batch normalization was incorporated after the second hidden layer. Batch normalization is a technique that normalizes the activations within a layer during training, which can help mitigate issues like internal covariate shift and accelerate convergence (Ioffe, 2015). The choice of the optimization method was the Adam optimizer, a powerful tool for training neural networks. It adaptively adjusted learning rates, thereby optimizing the learning process, and enabling rapid convergence while employing Mean Squared Error (MSE) as the loss function (Kingma & Ba, 2014). To prevent overfitting by the Adam optimizer, an early stopping mechanism was implemented. This mechanism continuously monitored the loss function for the hold out data during training, ceasing the process if no improvement or a sudden increase was detected over a predetermined number of consecutive epochs.

The initial deep neural networks (DNN) were configured with 4 input parameters and the daily logarithmic scaled matric potential (MP) value as output. The input parameters consisted of precipitation, potential evapotranspiration, measured VWC, and the weekly percentage change in VWC. As the prediction process progressed, two major issues were identified. Firstly, the influence of the VWC measurements on the training process was found to be predominant. Consequently, a decision was made to increase the weight of precipitation and potential evapotranspiration in the calculation process by incorporating three new input parameters: the weekly total precipitation and evapotranspiration (the sum of the current day and the preceding six days), along with the difference between these two new components. Secondly, the use of logarithmic scaled MP values was found to be highly sensitive to data availability. Therefore, a decision was made to retrain the model using absolute linear MP values (see Appendix B). In total, the final model was equipped with 7 input parameters to predict the absolute linear MP values for a given location. For each site, a site-specific DNN was built. The extent of the training data is predominantly influenced by site-specific characteristics. For instance, sites characterized by sandy soils necessitated a shorter training duration in contrast to sites with a higher clay content. Typically, the training dataset spanned a duration of 4 to 7 years. During this period, 70% of the data were randomly selected for training, while the remaining 30% were set aside as holdout data (Gholamy, et al., 2018). The extra years of data beyond the initial training period were reserved for validation purposes.

2.3 Autoencoder neural network

The autoencoder, consisting of an encoder and a decoder, is an unsupervised deep neural network that learns how to efficiently compress input data into a meaningful representation and subsequently reconstruct the original data from this compressed form (Chen & Guo, 2023). By connecting the encoder and decoder, the autoencoder effectively captures important patterns and variations present in the data, enabling comprehensive analysis and interpretation (Chen & Guo, 2023). In this study, an autoencoder neural network (figure 3) was built to analyze the measured VWC time series at 20 cm depth for the 9 sites.

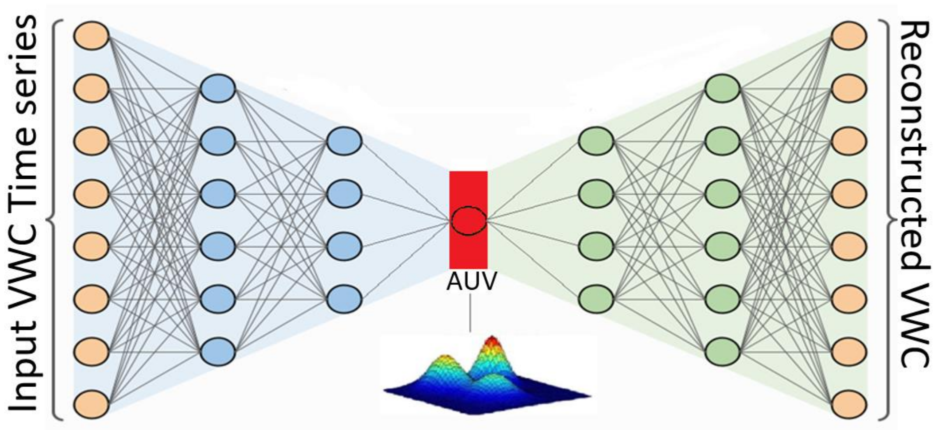

Figure 3 Autoencoder deep neural network for volumetric water content dynamic analysis. In this illustration, a densely connected autoencoder is utilized to compress the dynamic information of Volumetric Water Content (VWC) into a singular value, AUV, highlighted in red. The process begins with the encoder, depicted in blue, extracting the AUV from the measured volumetric water content time series (left orange layer). Subsequently, the densely connected decoder, represented in green, utilizes the AUV to reconstruct the VWC (orange layer at the right). Both the encoder and decoder, characterized by dense connections, optimized the AUV value by minimizing the error between the measured VWC and the reconstructed VWC.

The process was as follows. Firstly, an encoder neural network was created for each site. Its objective was to take the VWC time series as input and gradually reduce its dimensionality through hidden layers (Chen & Guo, 2023). The encoders' output was a single site-specific latent representation, called Autoencoder Value (AUV), and captures essential features of the VWC dynamics (Chen & Guo, 2023). Subsequently, a decoder neural network was developed to utilize the AUV value as reference to reconstruct the original VWC time series data. The success of this reconstruction depends on the training process, which aimed to optimize the AUV value by minimizing the error between the original VWC time series and its reconstructed counterpart by minimizing the mean squared error (MSE) value to less than 0.1.

After the optimization process, for each site one autoencoder value (AUV) was obtained. These AUV were scaled and then used to build a combined model (Figure 4) as follows. The AUV were sorted into three categories. Subsequently, one site from each category was selected. Finally, the data from the three chosen sites, each representing one category, were used to train the combined AUC-DNN model. The final combined model was thus equipped with 8 input parameters to predict the dynamic MP for a specific location. These parameters consisted of the same 7 inputs employed in the DNN model (section 2.2), complemented by the AUV. The neural network structure, as detailed in section 2.2, remained unchanged, employing the same optimization techniques.

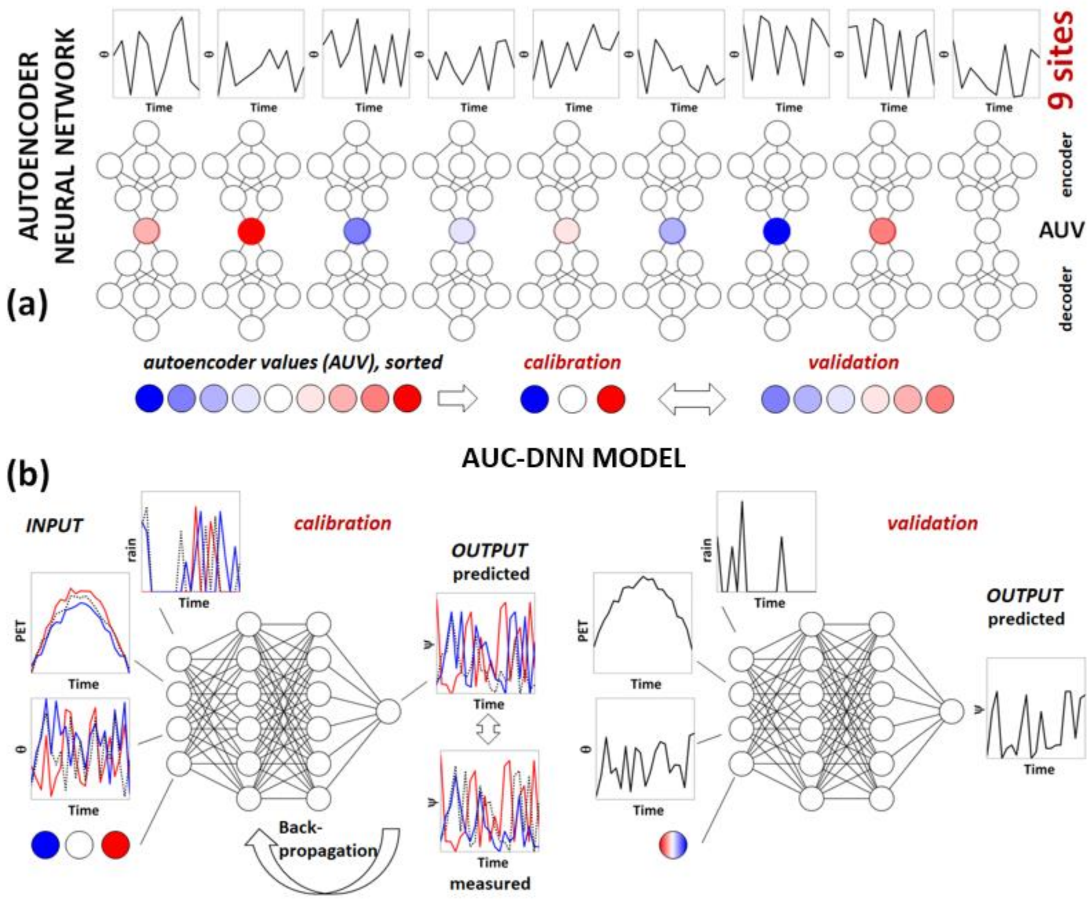

Figure 4 Application of two different types of deep neural network for the prediction of matric potential ψ. In this conceptual example, the water moisture dynamics of nine sites is considered. **(a)** The autoencoder neural network captures the characteristic features of the soil water content (θ) dynamics, assigning an autoencoder value (AUV) to each site. These values are sorted to AUV classes (one site from each class was used for calibration, remaining sites for validation). **(b)** The combined AUC-DNN model is built using the calibration sites with rainfall, potential evapotranspiration (PET), water content, and AUV as part of the 8-input parameters. The predicted matric potential (ψ) is compared to measured values for backpropagation. The calibrated DNN is then used to predict ψ for the remaining sites.

Initially, 70% of the data from each of the training sites were randomly selected for the training dataset. Subsequently, the remaining 30% of the data were set aside as the holdout dataset, serving as a benchmark for assessing model performance. The developed AUC-DNN was then applied for the other six sites (with the same input variables including AUV) to predict the entire datasets of those unseen sites. The combined model has thus the strengths of both components—the DNN' ability to understand dynamic MP patterns and the feature extraction capabilities of the autoencoder. This shift in the model's strength extends it from being site-specific to encompassing multiple sites, enabling it to gain a broader understanding of how the dynamic MP and AUV values relate.

2.4 Statistical evaluation

The evaluation of model performance is carried out by comparing the model predictions to the measured data. While there is no universal consensus on a standardized evaluation procedure, it is widely recognized that a multi-objective approach should be adopted e.g., (Boyle, et al., 2000; Willems, 2009). In this study, a combination of four evaluations tools was adopted. First, a scatter plot of observations against simulated values was utilized to visualize the degree of alignment with the identity line (often referred to as the 1:1 line). This graphical approach allowed for a qualitative assessment of model performance. A closer concentration of data points near the 1:1 line indicated higher agreement between calculated and observed values. Moreover, this graphical method includes the 95 % confidence interval area which help in scrutinizing the model's consistency across different prediction ranges and detecting potential biases within the model's performance (Ritter & Muñoz-Carpena, 2013).The second criterion evaluates the distribution of (signed) prediction errors (eq(2)). Ideally, the error distribution should be centered around zero, following a normal distribution pattern around this point with low standard deviation. Such a distribution indicates an unbiased model with errors that tend to balance out. Deviations from this pattern may suggest model bias or other unexpected characteristics in the prediction errors PE (Ouden, et al., 2012).

$$PE = O_i - P_i \tag{2}$$

with observed O_i and predicted matric potential value P_i. The third evaluation metric was the root means squared error (RMSE; eq (3a)). RMSE with a value of zero indicates perfect fit, while higher RMSE value means worse model performance (Ritter & Muñoz-Carpena, 2013). The final criterion for model evaluation involved the use of the dimensionless goodness-of-fit indicator (eq (3b)), known as the (Nash & Sutcliffe, 1970) coefficient of efficiency (NSE). NSE, which ranges from negative infinity to 1, serves as an indicator of model performance, with a value of 1 indicating a perfect fit, while a negative NSE suggests that using the means of the observed values is a better representative for the data than the evaluated model itself (Ritter & Muñoz-Carpena, 2013; Gupta & Kling, 2011). A NSE value > 0.75 indicates a very good model, while an NSE value < 0.5 signifies unsatisfactory results (Moriasi et al., 2007). In Gupta et al. (1999) a threshold NSE-value of 0.80 was used for good model performance and is applied here as well. The RMSE and NSE are defined by:

$$RMSE = \sqrt{\frac{\sum(O_i - P_i)^2}{N}} \tag{3a}$$

$$NSE = 1 - \frac{\sum(O_i - P_i)^2}{\sum(O_i - \bar{o})^2} \tag{3b}$$

where O_i represents the measured value, P_i the simulation output, and $\bar{o}$ the mean of the observed values, all within the context of a sample size N.

3. Results

Following the model discussion in section 2.2 and 2.3, we present first the results of the site-specific tests of predicting matric potential dynamics with a deep neural network (water content, rainfall and evapotranspiration as input data), before the role of autoencoder value is considered.

3.1 Deep neural network modeling without autoencoder

The site-specific DNN model was used to simulate the time series for all nine sites. In Figure 5, the results are shown for the Stüsslingen site (size #8, clay loam, meadow). The model was trained on data that had 1825 days of observations from January 2012 to January 2020. The data was split randomly into two parts: 1) a calibration dataset that had 1277 days and 2) a holdout dataset that had 548 days. The model was then validated on data from February 2018 to January 2023 (1379 days). A strong agreement between the model and the observed data was discovered in both the training and validation datasets (figure 5c) as reflected by the low RMSE value and the high NSE value (table 1). Furthermore, it was noticed that the error distribution exhibited a predominantly normal pattern with minimal bias towards higher observed values compared to the predicted values (figure 5d). These findings suggest that the site-specific DNN-model was not only able to be generalized well to unseen data but also demonstrated a reliable ability to predict MP.

The statistical evaluation (Table 1) reveals a consistent performance across both the training and validation periods for the Stüsslingen site, offering compelling evidence that the model avoids overfitting. Additionally, when it comes to predicting MP values, the 95 % confidence interval indicates that the model can capture well the overall dynamics (Figure 5b). However, the model performance exhibits higher deviations for values exceeding 400 cm and consistently underestimates values higher than 600 cm (figure 5b), which could explain the mild positive skewness observed in the distribution of prediction errors in figure 5d.

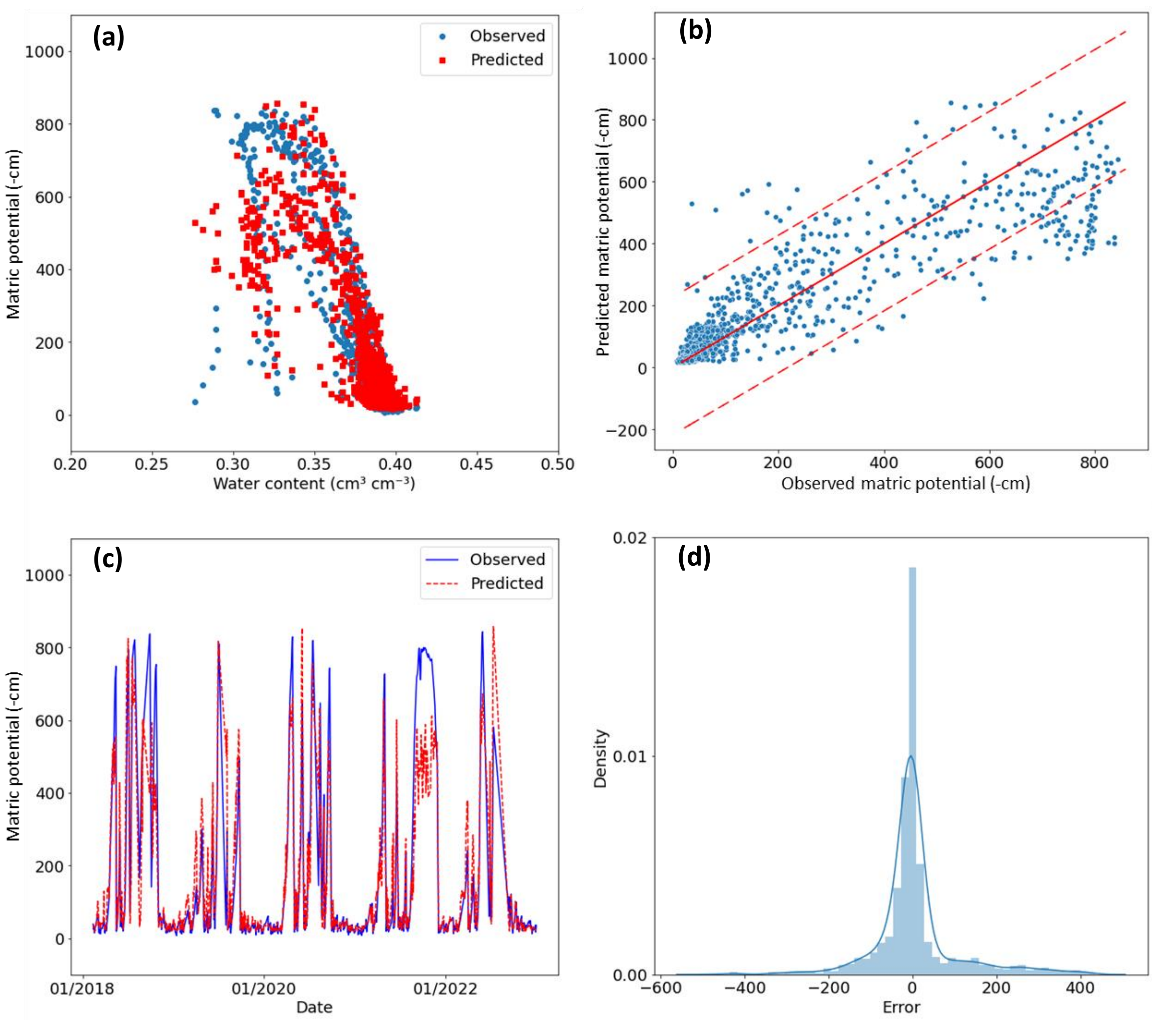

Figure 5 Graphical evaluation of the performance of the site-specific deep neural network (DNN) for validation for the Stüsslingen site (site #8) for the validation period 2018 to 2022. **(a)** Comparison between the simulated and measured soil water characteristics curve. **(b)** Scatter plot comparing simulated and measured matric potential values, providing a visual representation of the level of conformity to the identity line. The two dashed lines represent the 95% confidence interval around the identity line, providing a visual assessment of the level of agreement. **(c)** Model validation presenting time series with the observed and predicted matric potential. **(d)** Analysis of the distribution of prediction errors (observed minus predicted values) with positively mild skewed distribution

Comparing the performance for the 'holdout' period (randomly chosen days between 2012 and 2019) of the nine site-specific DNN models, the NSE index is larger than 0.55 ('good') for all and larger than 0.80 ('optimal) for six sites. For all sites it was thus possible to build a DNN model with good model performance for the randomly chosen test days. However, for the validation period, only four showed optimal performance (NSE > 0.80). For two forest sites with an optimal performance for the holdout period (Dulliken, site #4, and Etziken, site #5), the NSE dropped from a range between 0.82 and 0.88 to a range between 0.73 and 0.75 (table 1). Obviously, the model captured the overall short term dynamics during training (randomly chosen days) but faced problems in the precise prediction of the long validation period. An extended training period may be necessary to enhance the model's accuracy for these specific sites. Three grassland sites (Bellach, site #2, Matzendorf, #6, and Hofstetten-Flüh, #5) showed good but not optimal performance already during the holdout period. As discussed in the next section, this may be related to large variations of the pressure values for similar water contents and the corresponding large AUV. Notably, the lower performance observed in the holdout period for Hofstetten-Flüh could be also linked to data limitations, as only 1200 days were used to train the model for this specific site (compared to 1825 sites for the other sites).

Table 1 Statistical assessment of calibration (1825 days, until year 2019/2020) and validation results (years 2018/2019/2020 until years 2020/2021/2022) for nine sites. The holdout dataset was part of the training period and includes 548 days (30 % of calibration).

		Training (holdout)		**Validation**	
Location	AUV (-)	NSE (-)	RMSE (-cm)	NSE (-)	RMSE (-cm)
1 Aetigkofen	1.95	0.92	48	0.89	60
2 Bellach	7.00	0.70	98	0.62	125
3 Breitenbach[a, b]	3.56	0.86	82	0.83	96
4 Dulliken[a]	2.19	0.82	55	0.73	103
5 Etziken[a]	1.90	0.88	56	0.75	70
6 Hofstetten-Flüh[b]	5.59	0.76	90	0.63	123
7 Matzendorf	6.39	0.76	83	0.59	133
8 Stüsslingen	4.49	0.80	71	0.80	98
9 Zunzgen	6.44	0.87	62	0.83	73

[a] forest sites.
[b] Sites with limited available data. For those sites, only 1200 days were used for training; Within this training period, a subset of 360 randomly selected days was designated as a holdout dataset; the validation period for those specific sites was from 2018/2019 to 2022.

3.2 Autoencoder DNN

The Autoencoder values (AUV) deduced from the time series analysis of the volumetric water content for the period 2012-2022 can be classified in three main groups (figure 6). Soil water characteristics curves (SWC) with low water content at saturated conditions and a small variation of water content for similar potential values are assigned to ‘type 1’, contrasting ‘type 2’ with large water content values and variations. These types of SWC are related to small (‘type 1’) and high (‘type 2’) autoencoder values (AUV). Sites with AUV between these two classes, are denoted in the following as ‘transitional’ type. As shown in Table 1, the AUV of forest soils are small (mainly ‘type 1’) with large NSE values. In contrast to the forest soils, there are grassland sites with high AUV (‘type 2’) but small NSE. Probably, the high variations of the SWC curve for ‘type 2’ require longer training periods to capture the high variations in the pressure-saturation relationship.

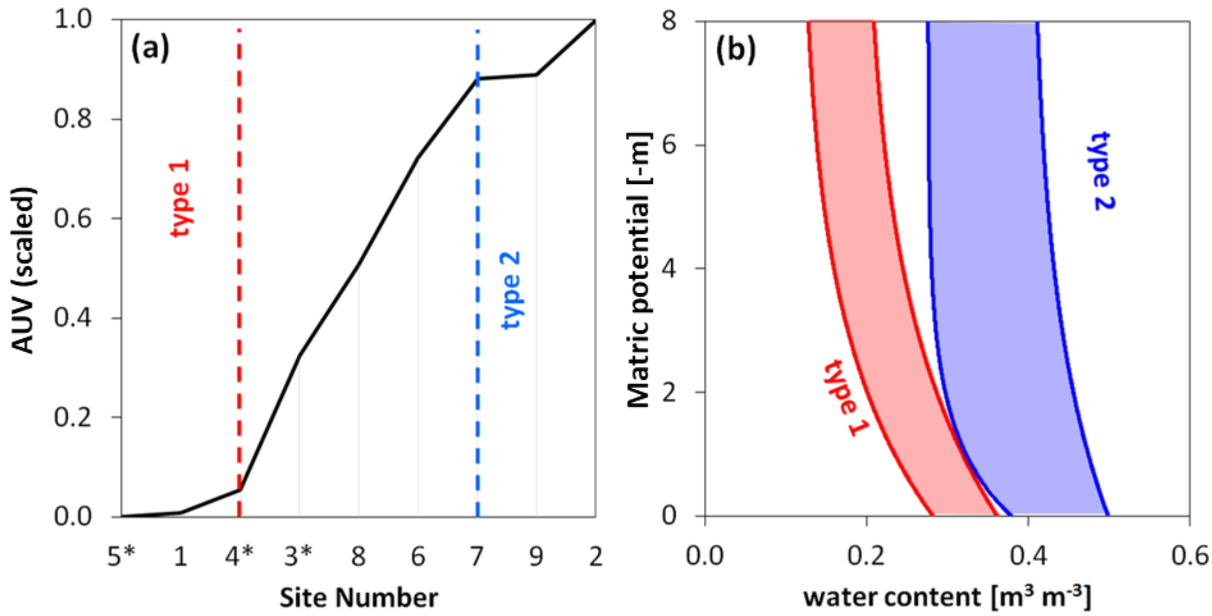

Figure 6 Autoencoder value (AUV) and its relation to the soil water characteristics curve (SWC). **(a)** The AUV of the nine sites with three sites of small (type 1) and three sites of high (type 2) AUV. **(b)** The type 1 of the SWC has small water contents close to saturation and a narrower range of water contents for similar water contents compared to type 2 with high water content values and variations. Type 1 shows the data range of Aetigkofen (site #1) and Type 2 for Bellach site (#2). The site numbers are chosen in alphabetic order and as shown in Figure 1 (Aetigkofen (1), Bellach (2), Breitenbach (3), Dulliken (4), Etziken (5), Hofstetten-Flüh (6), Matzendorf (7), Stüsslingen (8), Zunzgen (9); sites with forest are marked with *).

3.3 Deep neural network using the autoencoder value (AUC-DNN)

As mentioned in the previous section, the nine sites could be grouped into three main types according to the scaled autoencoder value (AUV). Consequently, it was assumed that the creation of a DNN model, which incorporates AUV in conjunction with the previously built site-specific neural network, could enable predictions for unseen sites. Ideally, the model should be trained with a balanced dataset, including one site from the ‘type 1’ category, one site from the ‘type 2’ category, and a few sites from the ‘transitional’ category to capture the full transition between the ‘type 1’ and ‘type 2’. However, due to the data limitation, the model was trained for only three sites representing the three types (Etziken, site #5, for 'type 1'; Bellach, #2, for 'type 2'; Stüsslingen, #8, for the 'transitional type') and was then used to predict the six unseen sites. The impact of the small training set (only one site for transitional type) was clear in the model results, which exhibited some instability, changing from one run to another as the model was not able to assume the same transitional function between sites consistently. Therefore, the model was run 20 times, then the average result for theses runs was taken as a representative outcome. The application of the new DNN model with AUV to predict the dynamic of matric potential is shown in Figure 7 for Breitenbach (site #3, loam, forest) as unseen site. The model was found to fell slightly behind the previously designed DNN model, but still can predict the dynamic in a good way. Notably, the NSE value for this model for Breitenbach site was 0.71 over the entire period from 2012 to 2022 (Table 2).

Table 2 AUC-DNN Model performance for the period 2012-2022. Three training sites were used to build the AUC-DNN model that was then applied for the other six sites. The sites are listed according to the corresponding autoencoder value (AUV). The asterisks mark the sites with forest; The AUV was scaled from 1.9 to 7.0 to simplify input. Alternatively, scaled values ranging from 0 to 1 could also be utilized.

Location	AUV	AUV (type)	used as	NSE (-)	RMSE
5 Etziken*	1.90	Type 1	Training site	0.82	70
1 Aetigkofen	1.95	Type 1	Validating site	0.76	88
4 Dulliken*	2.19	Type 1	Validating site	0.65	100
3 Breitenbach*	3.56	Transitional	Validating site	0.71	73
8 Stüsslingen	4.49	Transitional	Training site	0.85	116
6 Hofstetten-Flüh	5.59	Transitional	Validating site	0.60	113
7 Matzendorf	6.39	Type 2	Validating site	0.58	123
9 Zunzgen	6.44	Type 2	Validating site	0.69	104
2 Bellach	7.00	Type 2	Training site	0.71	104

It was noticed that the error distribution exhibited a predominantly normal pattern with a bias towards higher observed values compared to the predicted values (figure 7d). The analysis indicates the model's proficiency in forecasting dynamic trends rather than precise values (figure 7c). The results align with the anticipated scenario as the AUV for Breitenbach (3.56) was relatively close the Stüsslingen AUV value (4.49). Therefore, the underestimation detected in Stüsslingen for the site-specific DNN (figure 5b) is expected to exist in Breitenbach as well. The average model performance for all sites is presented in Table 2. The NSE values was > 0.55 for the 6 unseen sites (validating sites) and provided strong evidence that the model can be relied upon for the dynamic MP predictions.

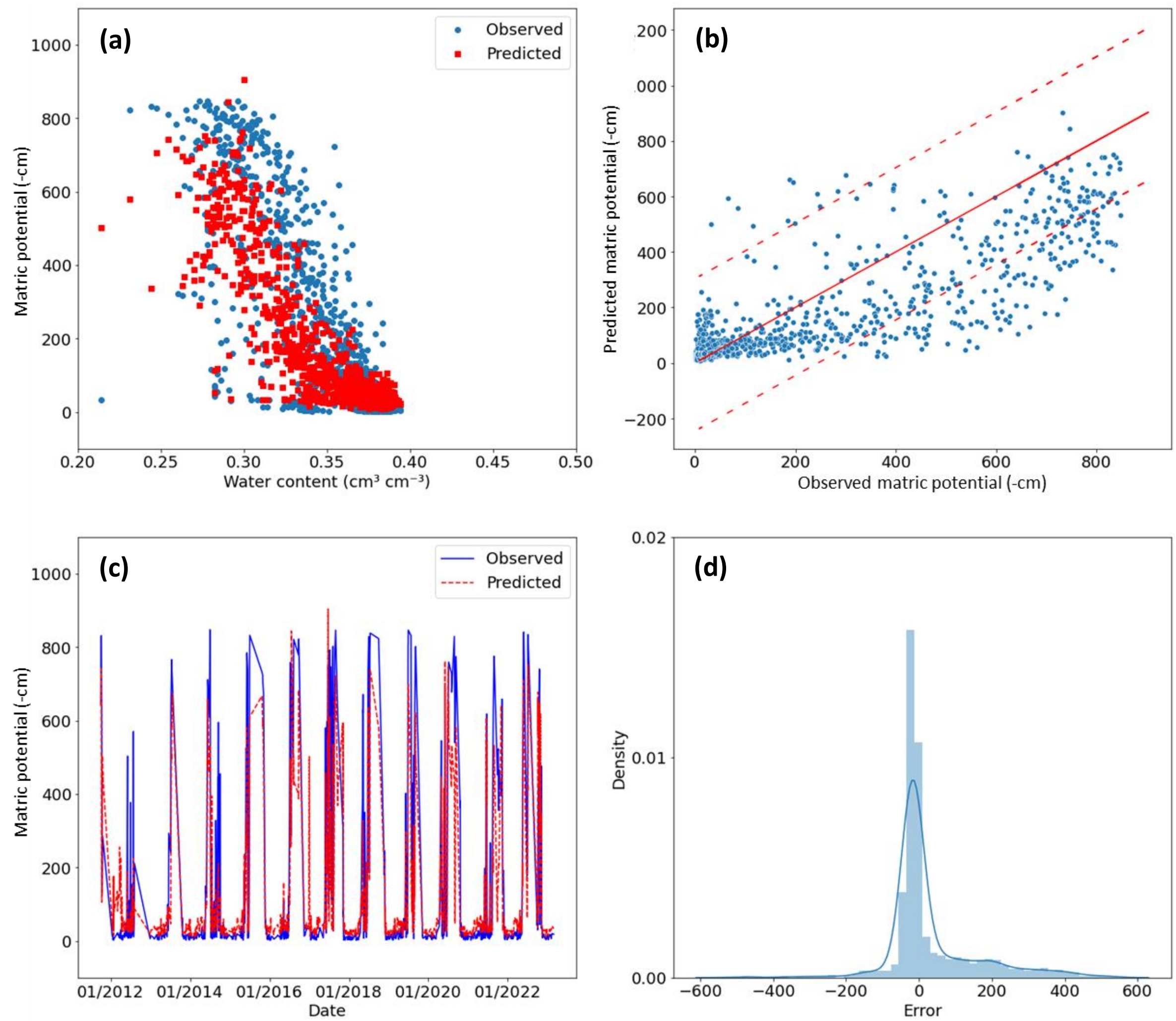

Figure 7 Evaluation of the Deep Neural Network with Autoencoder (AUC-DNN) model performance at the Breitenbach site for the period 2012-2022. **(a)** Comparison between the expected Soil Water characteristics curve (SWC) and the observed SWC. **(b)** Scatter plot that compares observed data points with their corresponding simulated values, providing a visual representation of the level of conformity to the identity line. The two dashed lines represent the 95% confidence interval around the identity line, providing a visual assessment of the level of agreement. **(c)** Time series comparison showing the observed and predicted matric potential for the entire period. **(d)** Analysis of the distribution of prediction errors (observed minus modelled value) using positively mild skewed distribution.

The NSE values for the unseen sites (validating sites) varied from 0.58 to 0.76, indicating a spectrum of model performance, ranging from acceptable to good. The low NSE values observed for Matzendorf (site #7) suggest that the model's utility is more suited for capturing overall trends and dynamics rather than precise values. This evaluation was further supported by examining a scatter plot (Figure 8) that compares the observed data points with their corresponding simulated values for the sites scored the lowest and the highest NSE, Matzendorf (site #7) and Aetigkofen (site #1). The plot revealed a wider 95% confidence interval for Matzendorf (figure 8a) in comparison to Aetigkofen (figure 8b), indicating that the lower the NSE value is, the more challenging it became for the model to predict the exact MP values. However, the model performance indicated the ability of the AUC-DNN model to predict dynamic MP without the necessity of site-specific training data, marking a transition from the DNN site-specific nature to a more versatile multi-site model.

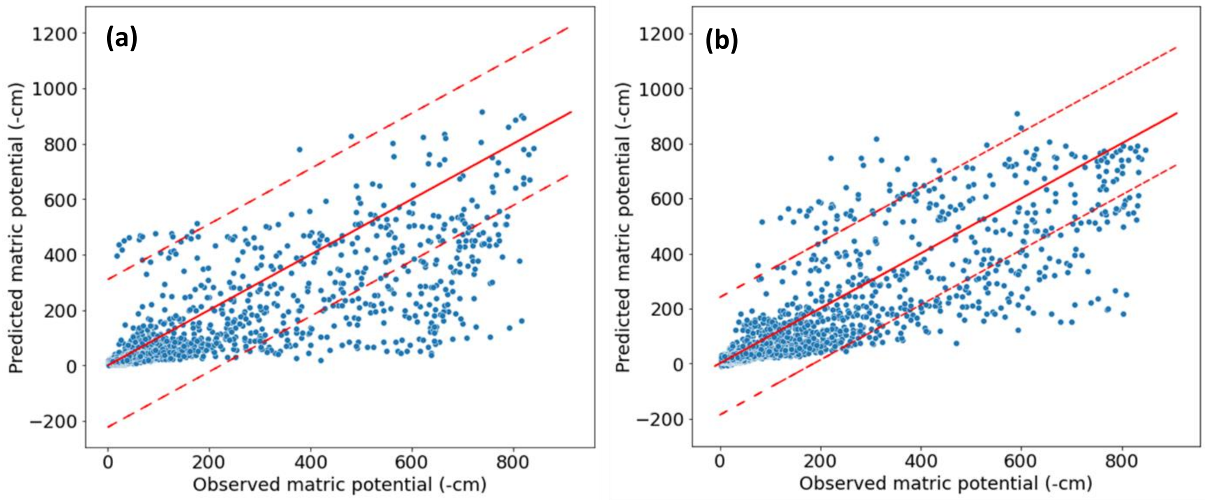

Figure 8 Comparison between observed data points and their corresponding simulated values for two sites with lowest and highest efficiency coefficient NSE. **(a)** Matzendorf (site #7) with NSE of 0.58. **(b)** Aetigkofen (site #1) with NSE of 0.76. The solid lines mark the 1:1 correspondence, the dashed lines the 95% confidence interval.

4. Discussion

Based on the analysis of the simulation results presented in section three, it can be asserted that the model was successfully built. However, as discussed in the next subsection, the model is expected to have certain drawbacks due to the limited number of available sites. In the other subsections, the relationship between the autoencoder value and soil properties and its application for satellite data will be discussed.

4.1 Limits of the deep neural network with autoencoder value (AUC-CNN)

First, the model's statistical evaluation revealed that the matric potential (MP) at a depth of 20 cm could be simulated with acceptable precision. However, a high variability in the evaluation is indicated by the NSE values for the unseen sites. This variance is attributed to the model's limited generalization capacity, as it was trained on just three sites. Furthermore, the model was not able to catch the whole dynamic for the training sites due to the limited length of available data. For example, Bellach (site #2), a training site that has a high AUV, had NSE value of 0.71 for the training period (table 2), which indicates that the model was able to catch the general trend for this site, but still can't predict the exact value of the MP. The effect of this result was obvious on the sites that are closed to AUV 'type two' category (e.g., Hofstetten-Flüh and Matzendorf, sites #6 and #7, with NSE of 0.60 and 0.58, respectively).

The stability of the AUC-DNN model was insufficient, as the model showed different prediction quality upon running the model repeatedly for the same training sites (figure 9). This variability in the outcomes indicates that the model can find different MP dynamics scenarios inside the training data. Therefore, it is recommended to train the model for more than one site in the same AUV type.

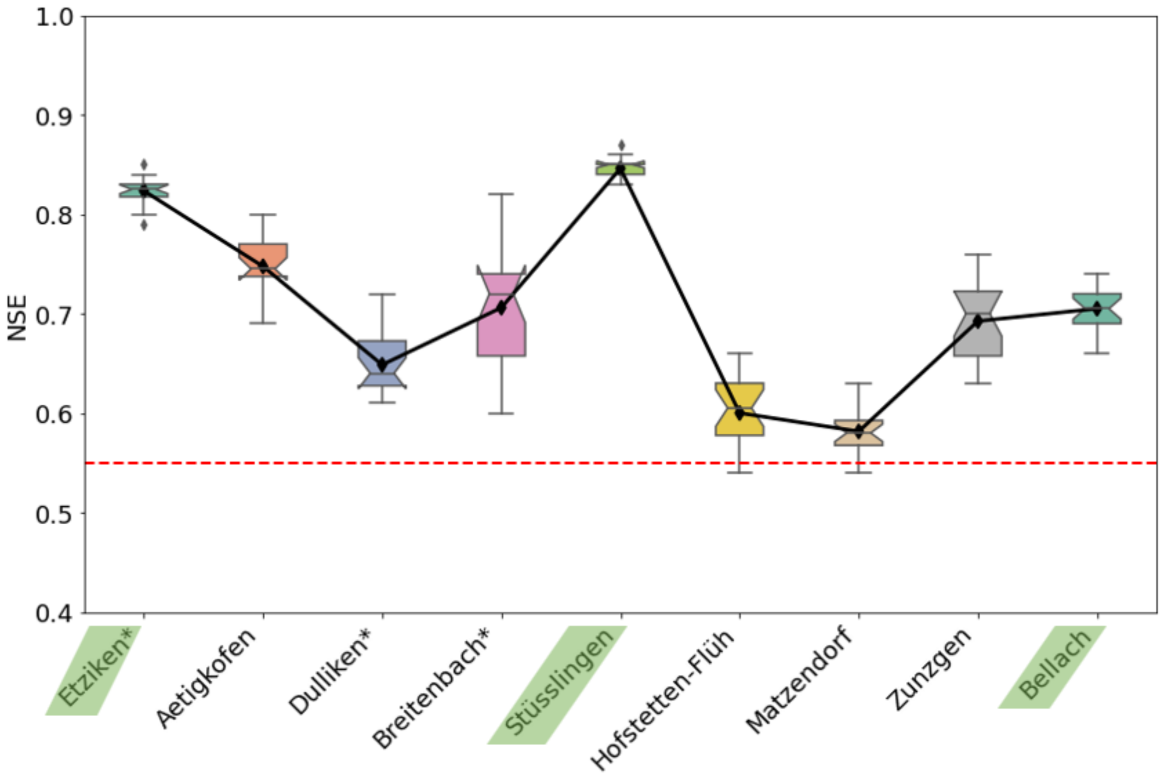

Figure 9 Variation of prediction results for 20 Runs for the AUC-DNN model quantified with the efficiency coefficient NSE. The highest variation was with the unseen sites in the transitional and type 2 categories. Each box represents the interquartile range, with the line inside denoting the median. The black diamond markers connect the mean values for each station, providing insight into the central tendency of the data. Notches on the boxplots offer a visual indication of the uncertainty around the median. The red dashed line represents the defined threshold for the NSE, set at 0.55 ; sites with forest are marked with *; training sites are highlighted in green.

Especially for the ‘transitional type’, choosing a site in the beginning, in between, and in the end of the category would stabilize the modeling results. However, in this study, there was no possibility to provide the model with extra data to solve the prediction instability. Therefore, a solution was implemented by 1) closely monitoring the model manually to ensure it captures the dynamic from all three sites. This involved training the model with nearly identical time periods for each site and visually confirming comprehensive coverage of the cloud of points for the retention curve of each site, avoiding concentration on specific patterns during training. The process also includes 2) running the model for 20 times, then averaging the results. Additionally, the statistical evaluation plots as shown in Figure 8, were used to detect instances with very low or very high MP prediction values.

For the set of sites analysed in this study, the model showed good generalization capacity and stability. However, the nine sites were similar with respect to climate and geology and the range of soil textural classes (see Figure 1) was relatively narrow. In a future study, the AUC approach will be applied for sites differing in climate and soil textural classes. We expect that the model can predict the dynamic matric potential for a new site as long as the autoencoder value falls within the range of AUV of the training sites. To predict the soil moisture dynamics for soils with autoencoder values outside of the range of training data, the model must be re-built using additional training data.

4.2 Interpretation of AUV and its relationship to physical soil properties

As discussed in section 3.2, the autoencoder value (AUV) is low for soil water characteristics curves (SWC) with low saturated water content and low variations of water content for a certain matric potential value (type 1) and high AUV for large values and variations of water content (type 2). To provide a more quantitative relationship between SWC and AUV, the SWC data were characterized as follows: the time average of volumetric water content (VWC) and SWP were calculated for 15 days for the period 2015 to 2022. The envelope of these data was then calculated by fitting a minimum and maximum pressure saturation relationship including the averaged data (see Figure 10a).

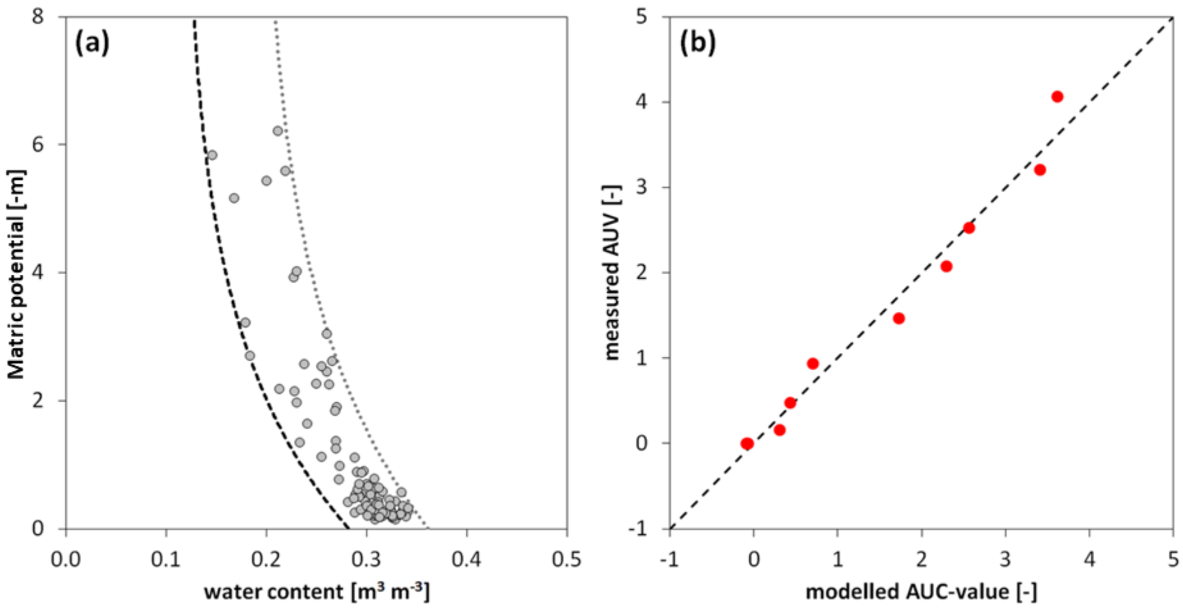

Figure 10 Relationship between autoencoder value (AUV) and soil water characteristics curve (SWC). **(a)** 15-days average of SWC data for Aetigkofen (symbols; site #1). The two lines are exponential functions building the envelope of the SWC curve. **(b)** Linear model for the nine sites linking the parameters of the exponential model with the 'measured' AUV (deduced from measured water content data).

The two boundary lines of the SWC were then characterized by a 'saturated' and 'residual' water content and a shape parameter defining an exponential decrease of water content with increasing absolute matric potential values. The SWC of each site can thus be described by six parameters (three parameters per boundary line). As shown in Figure 10b, a linear model expressing the AUV as function of these six parameters can be built. Simpler models with less parameters could not reproduce the AUV of all sites. Despite the positive correlation between AUV and average water content, the average water content alone is not sufficient to explain the range of AUV for all sites. Also combining average water content with soil texture information could not reproduce the AUVs of all sites, indicating that the soil moisture dynamics represented by AUV is not only dependent on static soil textural attributes but seasonal structural features as well.

Accordingly, there is no simple interpretation of AUV based on texture and average water content, but the dynamic variation of water content must be considered as well. Due to the relevance of the variation in water content for similar matric potential value, the use of a variational autoencoder (VAE) instead of the typical autoencoder could be considered. In contrast to the typical autoencoder that maps the input information into a single point (or a few points), the VAE produces a probability distribution capturing the variability (second moment) of the data. This could be specifically of interest for clay soils with high water contents (much larger than the residual water content) for the entire range of matric potential values. By including a probabilistic approach in the compressing and decompressing step, the variability of the data could be captured more efficiently using VAR.

4.3 Application for satellite data

The AUC-DNN model was used to analyze satellite-based volumetric water content (VWC) satellite data, including SMAP L4 and L3, SMOS products, and Sentinel data. Subsequently, a comparison was carried out for the AUV for both site-specific measurements and earth observation (EO) measurements for the same region. The initial findings highlighted a disparity between the dynamics captured by EO products and the actual dynamics. Therefore, if the objective is to establish a robust system capable of detecting changes in water retention dynamics on a regional scale, it is considered necessary to enhance the calibration of EO in Europe. Only with EO-data that can reproduce the essential of the soil moisture dynamics as manifested in the AUV, the matric potential dynamics can be deduced from EO-data. For future EO-data with improved capacity to capture regional soil moisture dynamics, the concept presented in this study (AUC-DNN) could be used to predict matric potential dynamics at global scale (see Appendix C).

5. Summary and conclusions

The soil water potential (SWP) determines water flow direction, water ability for plants, and mechanical stability. Because it cannot be measured directly by remote sensing techniques at larger scales, it is often deduced from water content information, assuming an unambiguous relationship between water content and SWP. However, this relationship under dynamic field conditions is highly ambiguous due to hysteresis, dynamic effects, and soil structural changes that cannot be modeled with a physically-based model. To enable prediction of SWP from soil water content, we apply a deep neural network (DNN) with an autoencoder to define unique features of the soil moisture dynamics. By inserting the autoencoder value (AUV) together with climatic data and water content measured at nine sites in the region of Solothurn (Switzerland) in a deep neural network (AUC-DNN), the soil water potential could be predicted. The main findings of the study can be summarized as follows:

- The SWC of the nine sites can be classified in three types based on the width of pressure-saturation relationship and the water content close to saturation
- These SWC-types are manifested in different autoencoder values (AUV)
- The AUV is not a simple function of average water content or soil texture but includes structural effects as well
- The AUC-DNN model could predict successfully the SWP dynamics of sites without site-specific training

The autoencoder value (AUV) is thus a new descriptor of the complex soil moisture dynamics that cannot be captured with physically based models. Future satellite generation may be sensitive enough to measure the AUV from remote sensing water content data. The approach presented in this paper will then enable the prediction of the soil matric potential at the global scale using remote sensing water content data.

Appendix A: Data Quality Assurance and Trend Analysis

As a precaution for data quality, the Absolute Matric Potential (AMP) and volumetric water content (VWC) data were scrutinized to identify potential errors the data. The process includes different steps that were necessary to discover anomalies, checking the integrity of the data, and detecting systematic changes with time.

1- Flagging Abrupt Changes in VWC and MP:

VWC Flagging and removing:

- Differences between consecutive (daily) time steps in the water content time series were calculated.
- Instances with daily differences exceeding 0.1 cm^3/cm^3 were flagged and denoted as sudden decreases or increases in VWC.

- Instances with VWC below 0.1 cm^3/cm^3 or exceeding 0.7 cm^3/cm^3 were identified and removed from the dataset. These extreme values were considered as measurement anomalies or outliers affecting the overall dataset's reliability.
- Instances with AMP<1 cm was removed from the data to overcome limitations in the used method. The water potential can change without modifying the volumetric water content after this limit, which could make the results of the model not accurate enough.
- The differences between consecutive time steps in AMP -time series was calculated; instances with daily differences exceeding 500 cm were flagged and called sudden decreases or increases in AMP (figure A1).
- The threshold AMP-value of 850 cm was employed in a specific step, where instances with AMP exceeding 850 cm were removed from the dataset, addressing the physical properties of water as it starts to boil in the tensiometers under pressure after this limit.
- Periods of concurrent decrease in AMP (indicator for wetting) and decrease in VWC (drying) were flagged (figure A1).
- Periods with matric potential values remaining constant over a three-day rolling window were flagged (figure A1).

2- Utilizing Index Windows for Data Manipulation and Data Removal

To address flagged instances mentioned before, a systematic approach is employed. For each flagged instance, three additional indices are generated around it to construct an index window, spanning one day before (index_1), the flagged instance itself (index_0), and two days after (index_2 and index_3). This four-day index window was eliminated from the dataset (figure A1). The decision to eliminate this window was informed by a visual assessment of measurements as it was noticed that when a measurement error occurs, the accuracy of the preceding day is affected. Furthermore, it was assumed that the device requires two subsequent days to restore normal measurement precision. This process contributes to a refined dataset, providing a more accurate representation of the underlying trends in AMP and VWC.

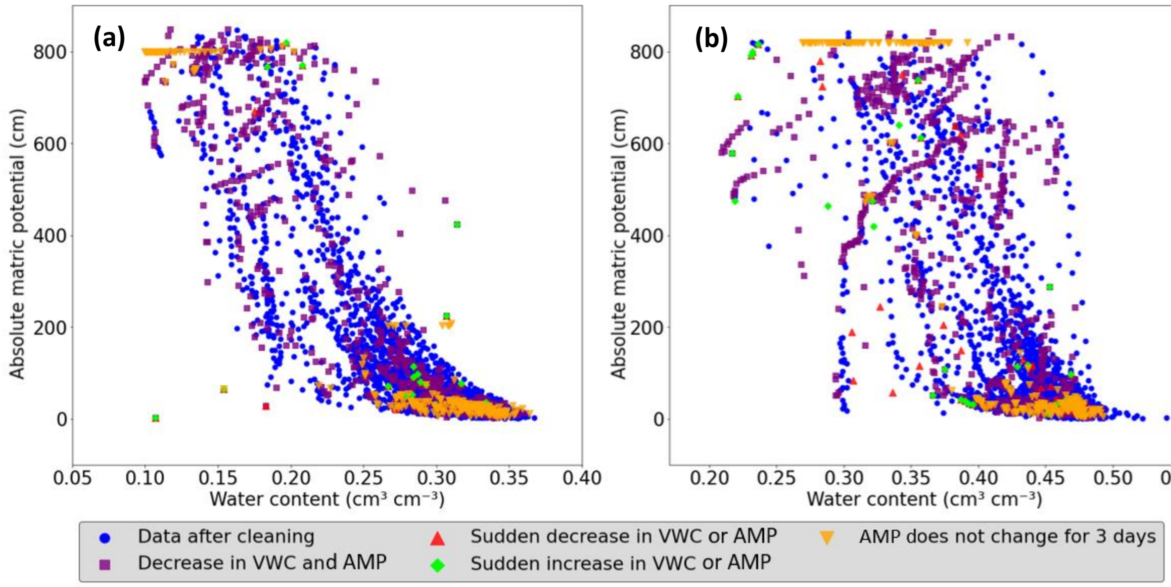

Figure A1 Comparison of data before and after cleaning procedure: the blue circles depict the remaining data after applying the cleaning criteria. Each distinct marker represents eliminated points, each corresponding to a specific criterion (e.g., the square purple marker for simultaneous decrease in volumetric water content (VWC) and the absolute matric potential (AMP), the red upward-pointing triangle is the marker for sudden decreases, the lime diamond for sudden increases, and the orange downward-pointing triangle marks periods of unchanged AMP). This provides insights into the reasons for data removal and illustrates the profound impact of the data cleaning process in retaining high-quality data points. In **(a)** the cleaning process for sandy clay loam site in Aetigkofen (site #1) is shown, in **(b)** the cleaning process for the Matzendorf site (site #9, clay loam soil).

Appendix B: Running the model with Logarithmic MP value.

The AUC-DNN showed a good performance in predicting the dynamic MP for the different 6 unseen sites. However, it was clear that the model prioritizes tends to focus on capturing significant changes in values rather than accurately representing the values themselves. This tendency is attributed to the substantial difference between the highest and lowest absolute values (approximately 850 cm), leading the model to emphasize major fluctuations while neglecting minor ones. To address this issue and enhance the model's precision in capturing the exact AMP, a suggestion has been made to train the model for the same three sites but with the logarithmic value for the AMP. This modification aims to strike a better balance, ensuring that both major and minor changes are effectively captured while maintaining accuracy in representing the specific values of MP.

To qualitatively assess the model training performance under the logarithmic scale, a scatter plot (Figure B1) was generated, comparing observations against simulated values for the second training site (Stüsslingen). The reason for choosing a training site was to understand how the model captures the dynamics when trained with logarithmic matric potential. The results suggest that using logarithmic scale, the model prioritized the prediction of the exact absolute value of matric potential (AMP), which makes the model to optimize predictions for the absolute values between 0 to 200 cm. This approach is giving the same importance to small and large changes in the AMP, which causes that the model assigned a higher weight to small changes according to their higher frequency, while neglecting less frequently occurring major dynamic shifts. Consequently, the model's accuracy went down beyond 200 cm (figure B1a) when compared to the model trained on non-logarithmic AMP-values (figure B1b). To maintain a balanced consideration of changes, logarithmic MP was avoided in the main part of the paper.

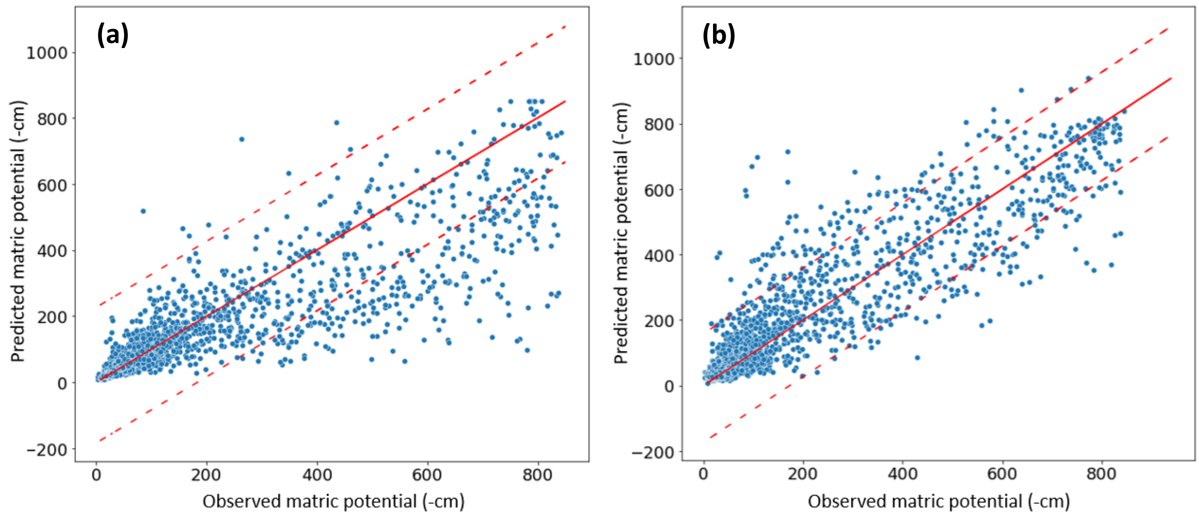

Figure B1 Visual comparison of model performance, comparing the observed and simulated values for the Stüsslingen training site. **(a)** the model trained with logarithmically scaled AMP-values, while in **(b)** The model trained with absolute linear matric potential (AMP) values. The solid line denotes the 1:1 correspondence, and dashed lines represent the 95% confidence interval.

Appendix C: SMAP data and Autoencoder for global scale analysis

SMAP (Soil Moisture Active Passive) is a NASA satellite mission that was established to help in improving weather forecasts and global drought monitoring. SMAP data products are available at different levels of processing, from Level 1 (L1; instrument measurements) to Level 4 (L4; model-derived value-added products). For this study, SMAP L3 and SMAP L4 products for measuring moisture content were used. The main difference between the two products is that SMAP L3 depends on the passive radiometer measurements, while SMAP L4 products are derived from a data assimilation system that combines the L-band brightness temperature observations from SMAP with a land surface model and meteorological forcing data (Reichle, et al., 2019). SMAP L3 products for moisture content are primarily affected by vegetation and surface roughness, allowing them to capture surface soil moisture variations. In contrast, the incorporation of land surface models in SMAP L4 products reduces its sensitivity to vegetation covers and surface roughness, making the products more representative of the profile soil moisture conditions (Reichle, et al., 2019; Ucla, Wood, & Sadri, 2018).

The autoencoder's encoded representations offer a unique opportunity to compare the spatial patterns inherent in "point measurement" with remote sensing data such as SMAP L3 and SMAP L4 data. The autoencoder method could illuminate how these diverse data streams align or diverge, providing crucial insights into the compatibility and complementarity of ground and satellite measurements. The process was applied for the data between the years 2015 to 2022. All the data (SMAP L4, SMAP L3, and on-site measurements) were given to the autoencoder neural network together. Subsequently, the resulting autoencoder values were scaled. Finally, a comparison was made to show if the satellite measurements and the on-site measurements have the same measured dynamics.

The autoencoder analysis of SMAP L3 (figure C1) indicates that satellite measurements struggle to capture the dynamic change of the water content, as all locations yield approximately the same Autoencoder Value (AUV). In contrast, the SMAP L4 product (figure C1) exhibits fluctuations in AUV results. For instance, Stüsslingen and Matzendorf align closely with on-site measurements in terms of AUVs. However, for Hofstetten-Flüh, the SMAP L4 product indicates a very small AUV, suggesting an expected dynamic in line with a type 1 soil water retention curve (figure 6b). In contrast, on-site measurements indicate a higher AUV for Hofstetten-Flüh, suggesting a closer association with a type 2 soil water retention curve. These findings underscore the imperative for developing a new methodology to calibrate satellite data in the Switzerland area. The prevalent uniformity in SMAP L3 results and the notable disparities between on-site measurements and satellite data across various products highlight the need for a more refined approach to ensure accurate and reliable dynamic soil moisture assessments.

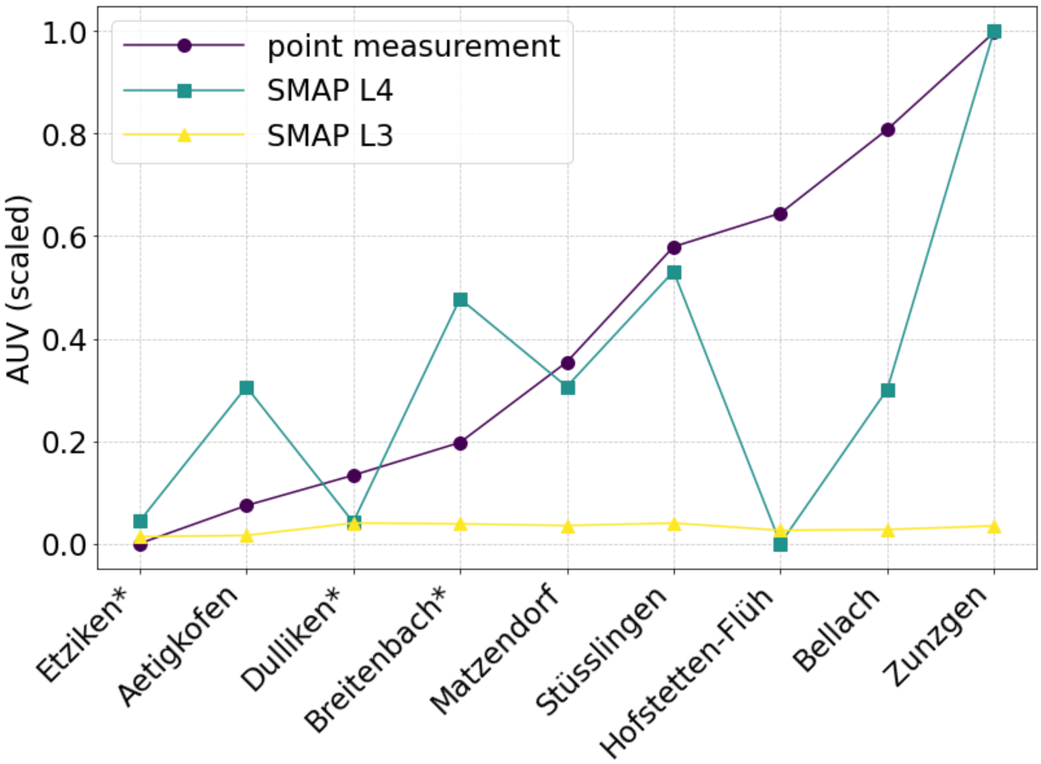

Figure C1 Comparative analysis of Autoencoder Neural Network results for SMAP L3 and SMAP L4 satellite data, alongside with profile measurements. The fluctuating AUV values indicate varying degrees of alignment with on-site measurements across different locations. Sites with forest are marked with *.

Code and data availability

The related input data for the AUC-DNN model and Python code are openly accessible under https://doi.org/10.5281/zenodo.10600669 and https://doi.org/10.5281/zenodo.10602397 respectively. The input for the autoencoder and its python codes are openly accessible under https://www.doi.org/10.5281/zenodo.10605108

Author contributions

NA, AC, and PL designed the research. NA and PL performed the research. NA and MR analyzed the soil moisture time series. SM was responsible for the soil moisture network. NA wrote the codes and built the model. NA and PL wrote the manuscript with substantial input from all co-authors.

Competing interests

The contact author has declared that none of the authors has any competing interests.

Financial support

"This research is part of the project Artificial Intelligence for Soil Health. Funded by the European Union. Views and opinions expressed are however those of the author(s) only and do not necessarily reflect those of the European Union or of the Research Executive Agency (REA). Neither the European Union nor the granting authority can be held responsible for them."

Acknowledgements

NA acknowledges the utilization of ChatGPT to enhance coherence within certain sections of the manuscript.

References

Achieng, K. O. (2019). Modelling of soil moisture retention curve using machine learning techniques: Artificial and deep neural networks vs support vector regression models. Computers & Geosciences, 133, 104320. https://doi.org/10.1016/j.cageo.2019.104320

Basile, A., Bonfante, A., Coppola, A., De Mascellis, R., Falanga Bolognesi, S., Terribile, F., & Manna, P. (2019). How does PTF Interpret Soil Heterogeneity? A Stochastic Approach Applied to a Case Study on Maize in Northern Italy. *Water*, *11*(2), 275. https://doi.org/10.3390/w11020275

Bertels, D., & Willems, P. (2023). Physics-informed machine learning method for modelling transport of a conservative pollutant in surface water systems. *Journal of Hydrology*, *619*, 129354. https://doi.org/10.1016/j.jhydrol.2023.129354

BODENMESSNETZ: https://www.bodenmessnetz.ch/, last access: 20 January 2024.

Boyle, D. P., Gupta, H. V., & Sorooshian, S. (2000). Toward improved calibration of hydrologic models: Combining the strengths of manual and automatic methods. *Water Resources Research*, *36*(12), 3663–3674. https://doi.org/10.1029/2000WR900207

Bundesamt für Energiewirtschaft. (1997). Richtlinien zum Schutze des Bodens beim Bau unterirdisch verlegter Rohrleitungen (Bodenschutzrichtlinien). Bundesamt für Energiewirtschaft. Schweiz: Bundesamt für Energiewirtschaft.

Capparelli, G., & Spolverino, G. (2020). An Empirical Approach for Modeling Hysteresis Behavior of Pyroclastic Soils. *Hydrology*, *7*(1), 14. https://doi.org/10.3390/hydrology7010014

Chen, S., & Guo, W. (2023). Auto-Encoders in Deep Learning—A Review with New Perspectives. *Mathematics*, *11*(8), 1777. https://doi.org/10.3390/math11081777

D. N. Moriasi, J. G. Arnold, M. W. Van Liew, R. L. Bingner, R. D. Harmel, & T. L. Veith. (2007). Model Evaluation Guidelines for Systematic Quantification of Accuracy in Watershed Simulations. *Transactions of the ASABE*, *50*(3), 885–900. https://doi.org/10.13031/2013.23153

den Ouden, H. E. M., Kok, P., & de Lange, F. P. (2012). How Prediction Errors Shape Perception, Attention, and Motivation. *Frontiers in Psychology*, *3*. https://doi.org/10.3389/fpsyg.2012.00548

Fomin, D. S., Yudina, A. V., Romanenko, K. A., Abrosimov, K. N., Karsanina, M. V., & Gerke, K. M. (2023). Soil pore structure dynamics under steady-state wetting-drying cycle. *Geoderma*, *432*, 116401. https://doi.org/10.1016/j.geoderma.2023.116401

Fu, Y. P., Liao, H. J., Chai, X. Q., Li, Y., & Lv, L. L. (2021). A Hysteretic Model Considering Contact Angle Hysteresis for Fitting Soil-Water Characteristic Curves. *Water Resources Research*, *57*(4). https://doi.org/10.1029/2019WR026889

Gallipoli, D., Gens, A., Sharma, R., & Vaunat, J. (2003). An elasto-plastic model for unsaturated soil incorporating the effects of suction and degree of saturation on mechanical behaviour. *Géotechnique*, *53*(1), 123–135. https://doi.org/10.1680/geot.2003.53.1.123

Gholamy, A., Kreinovich, V., & Kosheleva, O. (2018). Why 70/30 or 80/20 Relation Between Training and Testing Sets:. Texas: Departmental Technical Reports (CS), University of Texas at El Paso. https://scholarworks.utep.edu/cgi/viewcontent.cgi?article=2202&context=cs_techrep

Gupta, H. V., & Kling, H. (2011). On typical range, sensitivity, and normalization of Mean Squared Error and Nash-Sutcliffe Efficiency type metrics. *Water Resources Research*, *47*(10). https://doi.org/10.1029/2011WR010962

Gupta, H. V., Sorooshian, S., & Yapo, P. O. (1999). Status of Automatic Calibration for Hydrologic Models: Comparison with Multilevel Expert Calibration. *Journal of Hydrologic Engineering*, *4*(2), 135–143. https://doi.org/10.1061/(ASCE)1084-0699(1999)4:2(135)

Gupta, S., Lehmann, P., Bickel, S., Bonetti, S., & Or, D. (2023). Global Mapping of Potential and Climatic Plant-Available Soil Water. *Journal of Advances in Modeling Earth Systems*, *15*(11). https://doi.org/10.1029/2022MS003277

Hannes, M., Wollschläger, U., Wöhling, T., & Vogel, H. -J. (2016). Revisiting hydraulic hysteresis based on long-term monitoring of hydraulic states in lysimeters. *Water Resources Research*, *52*(5), 3847–3865. https://doi.org/10.1002/2015WR018319

Holthusen, D., Peth, S., & Horn, R. (2010). Impact of potassium concentration and matric potential on soil stability derived from rheological parameters. *Soil and Tillage Research*, *111*(1), 75–85. https://doi.org/10.1016/j.still.2010.08.002

IDAweb: https://Gate.Meteoswiss.Ch/Idaweb/PrepareRegistration.Do/, last access: 20 January 2024

Ioffe, S., & Szegedy, C. (2015). Batch Normalization: Accelerating Deep Network Training by Reducing Internal Covariate Shift. http://arxiv.org/abs/1502.03167

Jain, S. K., Singh, V. P., & van Genuchten, M. Th. (2004). Analysis of Soil Water Retention Data Using Artificial Neural Networks. *Journal of Hydrologic Engineering*, *9*(5), 415–420. https://doi.org/10.1061/(ASCE)1084-0699(2004)9:5(415)

Kingma, D. P., & Ba, J. (2014). *Adam: A Method for Stochastic Optimization*. http://arxiv.org/abs/1412.6980

Lu, L. (2020). Dying ReLU and Initialization: Theory and Numerical Examples. *Communications in Computational Physics*, *28*(5), 1671–1706. https://doi.org/10.4208/cicp.OA-2020-0165

Lu, N., Godt, J. W., & Wu, D. T. (2010). A closed-form equation for effective stress in unsaturated soil. *Water Resources Research*, *46*(5). https://doi.org/10.1029/2009WR008646

Ma, Y., Liu, H., Yu, Y., Guo, L., Zhao, W., & Yetemen, O. (2022). Revisiting Soil Water Potential: Towards a Better Understanding of Soil and Plant Interactions. *Water*, *14*(22), 3721. https://doi.org/10.3390/w14223721

Mendes, J., & Buzzi, O. (2013). New insight into cavitation mechanisms in high-capacity tensiometers based on high-speed photography. *Canadian Geotechnical Journal*, *50*(5), 550–556. https://doi.org/10.1139/cgj-2012-0393

Menon, M., Mawodza, T., Rabbani, A., Blaud, A., Lair, G. J., Babaei, M., Kercheva, M., Rousseva, S., & Banwart, S. (2020). Pore system characteristics of soil aggregates and their relevance to aggregate stability. *Geoderma*, *366*, 114259. https://doi.org/10.1016/j.geoderma.2020.114259

Montesinos López, O. A., Montesinos López, A., & Crossa, J. (2022). Fundamentals of Artificial Neural Networks and Deep Learning. In *Multivariate Statistical Machine Learning Methods for Genomic Prediction* (pp. 379–425). Springer International Publishing. https://doi.org/10.1007/978-3-030-89010-0_10

Nash, J. E., & Sutcliffe, J. V. (1970). River flow forecasting through conceptual models part I — A discussion of principles. *Journal of Hydrology*, *10*(3), 282–290. https://doi.org/10.1016/0022-1694(70)90255-6

Rawls, W. J., Pachepsky, Y. A., Ritchie, J. C., Sobecki, T. M., & Bloodworth, H. (2003). Effect of soil organic carbon on soil water retention. *Geoderma*, *116*(1–2), 61–76. https://doi.org/10.1016/S0016-7061(03)00094-6

Reichle, R. H., Liu, Q., Koster, R. D., Crow, W. T., De Lannoy, G. J. M., Kimball, J. S., Ardizzone, J. V., Bosch, D., Colliander, A., Cosh, M., Kolassa, J., Mahanama, S. P., Prueger, J., Starks, P., & Walker, J. P. (2019). Version 4 of the SMAP Level-4 Soil Moisture Algorithm and Data Product. *Journal of Advances in Modeling Earth Systems*, *11*(10), 3106–3130. https://doi.org/10.1029/2019MS001729

Ritter, A., & Muñoz-Carpena, R. (2013). Performance evaluation of hydrological models: Statistical significance for reducing subjectivity in goodness-of-fit assessments. *Journal of Hydrology*, *480*, 33–45. https://doi.org/10.1016/j.jhydrol.2012.12.004

Romero-Ruiz, A., Linde, N., Keller, T., & Or, D. (2018). A Review of Geophysical Methods for Soil Structure Characterization. *Reviews of Geophysics*, *56*(4), 672–697. https://doi.org/10.1029/2018RG000611

Ross, P. J., & Smettem, K. R. J. (2000). A Simple Treatment of Physical Nonequilibrium Water Flow in Soils. *Soil Science Society of America Journal*, *64*(6), 1926–1930. https://doi.org/10.2136/sssaj2000.6461926x

Rostami, A., Habibagahi, G., Ajdari, M., & Nikooee, E. (2015). Pore Network Investigation on Hysteresis Phenomena and Influence of Stress State on the SWRC. *International Journal of Geomechanics*, *15*(5). https://doi.org/10.1061/(ASCE)GM.1943-5622.0000315

Sadeghi, H., Chiu, A. C. F., Ng, C. W. W., & Jafarzadeh, F. (2018). A vacuum-refilled tensiometer for deep monitoring of in-situ pore water pressure. *Scientia Iranica*, 1–19. https://doi.org/10.24200/sci.2018.5052.1063

Shwetha, P., & Varija, K. (2015). Soil Water Retention Curve from Saturated Hydraulic Conductivity for Sandy Loam and Loamy Sand Textured Soils. *Aquatic Procedia*, *4*, 1142–1149. https://doi.org/10.1016/j.aqpro.2015.02.145

Smith, C. W., Johnston, M. A., & Lorentz, S. A. (2001a). The effect of soil compaction on the water retention characteristics of soils in forest plantations. *South African Journal of Plant and Soil*, *18*(3), 87–97. https://doi.org/10.1080/02571862.2001.10634410

Smith, C. W., Johnston, M. A., & Lorentz, S. A. (2001). The effect of soil compaction on the water retention characteristics of soils in forest plantations. *South African Journal of Plant and Soil*, *18*(3), 87–97. https://doi.org/10.1080/02571862.2001.10634410

Spreafi, M., & Weingartner, R. (2005). The Hydrology of Switzerland Selected aspects and results. In *Reports of the FOWG, Water Series* (Issue 7). www.bbl.admin.ch/bundespublikationen

Tuller, M., & Or, D. (2023). Soil water retention and characteristic curve. In *Encyclopedia of Soils in the Environment* (pp. 187–202). Elsevier. https://doi.org/10.1016/B978-0-12-822974-3.00105-1

Ucla, S. S., Wood, E. F., & Sadri, S. (2018). *A SMAP-Based Drought Monitoring Index for the United States*. https://doi.org/10.5194/hess-2018-182

Willems, P. (2009). A time series tool to support the multi-criteria performance evaluation of rainfall-runoff models. *Environmental Modelling & Software*, *24*(3), 311–321. https://doi.org/10.1016/j.envsoft.2008.09.005

Zuo, Y., & He, K. (2021). Evaluation and Development of Pedo-Transfer Functions for Predicting Soil Saturated Hydraulic Conductivity in the Alpine Frigid Hilly Region of Qinghai Province. *Agronomy*, *11*(8), 1581. https://doi.org/10.3390/agronomy11081581